Experimental investigation of multi-physics control of a two-fluid coaxial atomizer

N. Machicoane*, R. Osuna-Orozco, P.D. Huck, A. Aliseda
Department of Mechanical Engineering, University of Washington, USA

Abstract

We investigate multiphysics control strategies on the atomization of a laminar liquid round jet by a turbulent coaxial gas jet. Spray control (i.e. driving the spatio-temporal distributions of droplet size and number density towards a desired objective) requires a mechanistic understanding of the processes that control droplet formation and transport: primary and secondary instabilities, turbulent transport, forces on the droplets, .etc. We present the experimental characterization of the break-up dynamics in a canonical coaxial atomizer in a series of open loop conditions with harmonic forcing of the gas swirl ratio and liquid injection rate. Low frequency harmonic modulation of the liquid and gas flow rates are investigated. Time resolved measurements of the spray structure, as well as the droplet size and velocity are provided. The effect of actuation is characterized for different gas momentum ratios ranging from 5 to 75. This open-loop characterization of the injector will be used to develop reduced order models for feedback control, as well as to validate assumptions underlying an adjoint-based computational control strategy. This work is part of a large-scale project funded by an ONR MURI to provide fundamental understanding of the mechanisms for feedback control of sprays.

Introduction

Liquid sprays are involved in many environmental phenomena (e. g. ocean sprays) and engineering processes (e. g. fuel sprays for combustion, coating). Active control of such multi-phase flows has not been tackled yet despite the direct applications involved (spray control is defined here as actuation that drives the droplet size and spatial distributions towards a desired state). Open loop actuation strategies for coaxial two-fluid atomizers have been investigated in the literature, using swirling motion in the gas co-flow [1] or an external acoustic field acting on the spray [2]. We study multi-physics perturbations in a canonical geometry, beginning with open loop fluctuations, and characterize the transfer function from inputs to spray state with the aim to develop a reduce-order model for feedback control implementation. The perturbations discussed here are a time-dependent modulation of swirling motions of the gas co-flow and the application of an external electric field to change the spatial distribution of the droplets.

Experimental Methods

Experimental setup

A two-fluid coaxial atomizer has been designed to study atomization physics in a canonical setting. The design focuses on obtaining well-characterized and reproducible laminar liquid and turbulent gas streams. The liquid is introduced via a straight circular duct. Fully developed Poiseuille flow is found at the outlet of the liquid nozzle, into the atomization process. The gas enters the nozzle through its sidewalls, perpendicular to the axis of the gas nozzle through eight inlets (four on-axis inlets for the no-swirl gas feed, and four off-axis inlets to induce angular momentum on the swirl gas feed). The gas then flows longitudinally along the axis of the injector forming a nozzle whose inner (the outer wall of the liquid needle) and outer surfaces are cubic-spline shaped (see [3] for more details on the design and the atomizer characterization). This canonical configuration is also investigated by our team using radiographic measurements [4, 5, 6] and computational simulations [7]

The gas swirl flow rate, which is then split into the 4 swirl inlet into the nozzle, is controlled through an electro-valve that allows for modulations of the flow rate on periods of the order of one second. When swirl is added to the gas co-flow, the total gas flow rate (hence the momentum gas-to-liquid flux ratio M) is kept constant, diverting part of the total gas from the no-swirl line to the swirl line, so that we use the swirl ratio SR to characterize the effect of this input into the spray dynamics. This ratio compares the flow rate of swirled gas to the no-swirl gas flow rate. The gas-to-liquid momentum ratio $M = \rho_g U_g^2/\rho_l U l^2$ is based on the total gas and liquid average velocities and densities at the nozzle exit, $U_i = Q_i/A_i$ and ρ_i, where the subscripts g and l are used for gas an liquid respectively in the following, and A is the fluid area.

The liquid needle is connected to a negative electric potential (-5 kV) and a ground electrode is placed coaxially with the liquid anode at the exit of the gas nozzle. Thus, a large electric charge ($\approx 0.1 - 1\ C/Kg$) is transferred

*Corresponding author: nmachico@uw.edu

Figure 1. Schematics of the canonical coaxial two-fluid atomizer. The potential V_1 is set at -5 kV to charge the liquid, while the plate configuration can be $V_2 = V_3 = 0$ for outward electric forcing, $V_2 = V_3 = -5$ kV for an inward electric forcing and $V_2 = -5$ kV and $V_3 = 0$ for an upward electric forcing.

to the dielectric liquid (distilled, reversed-osmosis, water) when it flows through the strong electric field that exists at the nozzle exit. Large parallel metallic plates are placed downstream of the nozzle as sketched in figure 1. Each plate can either be set to the same potential as the needle or can be grounded, so the resulting electric field set between the plates and the nozzle electrodes create different forces on the negatively charged droplets.

High-speed shadowgraphy

The different modes of atomization accessible for study in this coaxial two-fluid atomizer are mapped via high-speed flow visualization in this paper. Specifically, a range of gas Reynolds numbers from 10^4 to 2 10^5 has been explored, keeping the liquid Reynolds number constant at 1000 to maintain laminar conditions inside the liquid injection needle up to the nozzle, resulting in gas-to-fluid momentum ratio ranging from $M = 0.9$ to 80. The Reynolds number is defined as $Re_i = 2Q_i/\sqrt{piA_i}\nu_i$, with Q and ν being the flow rate and the kinematic viscosity respectively. The Weber number ($We = \rho_g U_g^2 d_l/\sigma$) range explored, based on the gas exit velocity and liquid jet diameter d_l is $10 - 10^4$ [8].

Shadowgraphy high speed movies (912×912 pixels acquired at 10,000 frames per second, with 0.285 ns exposure time) allow for a qualitative mapping of the different instabilities and atomization modes [9]. At low gas Reynolds, $Re_g = 10^4$, and momentum ratio values, $M = 5$, a sinusoidal instability (referred to in the following as flapping) exposes the liquid jet to the high speed gas and results in multi-bag break up. At intermediate gas Reynolds numbers, the liquid jet accelerates, narrowing sharply within the potential cone of the gas, and suffers from a symmetric varicose instability that exposes the liquid to the high speed gas, with further instability forming ligaments and leading to break up into droplets [10]. For the highest gas Reynolds numbers ($Re_g > 10^5$, $M > 70$), the liquid-gas interface is subject to the classical Kelvin-Helmhotz instability, the ligaments formed by this instability quickly accelerate, become subject to a Raleigh-Taylor type instability and break into individual droplets [11].

Results and Discussion

We characterize the primary break-up instability using power spectral densities of the pixel intensity of a cross-stream half-line placed a few liquid diameters downstream of the injection. When the sum of the pixel intensities along a half-width line is considered, the flapping motions of the liquid core can be observed from drastic changes of this quantity over time, that highlight the changes in droplet size and number density that flow across the two image halves. Its power spectral density (PSD) effectively identifies peaks at the frequencies associated with spray structures (figure 2). The phase correlation between the signals from the two image halves allows for identification of the liquid primary instability mode (sinusoidal, 180° phase lag, or varicose, 0° phase lag between the halves). At low momentum ratio values, the peak is well defined and harmonics are present, moving to higher frequency values and broadening for higher M. Figure 3 shows the evolution of this flapping frequency with M, which is well approximated by a power law of exponent 0.7. When a steady swirl is introduce (for $M = 6$), the flapping frequency is increased by approximately 30%, while swirling motions modulated at a period of 1.5 s actually decreased it by 25%.

While shadowgraph high-speed movies are not suitable to measure the droplet size distribution after the sec-

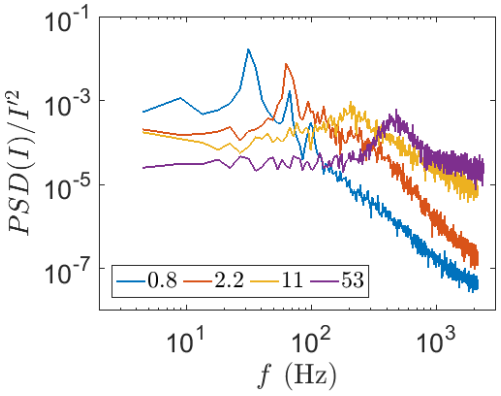

Figure 2. Power spectral density (PSD) of the pixel intensity summed along a cross-stream line for different values of the momentum ratio M, showing peaks at the flapping frequency.

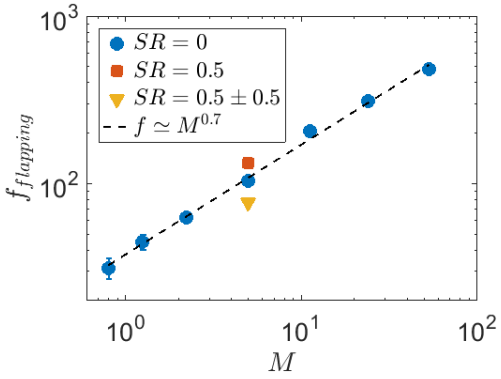

Figure 3. Flapping frequency, defined as the peak of the PSD from figure 2, as a function of the momentum ratio M in the absence of swirl $\circ$, for a fixed swirl ratio $SR = 0.5$ $\square$ and for a swirl ratio modulated from 0 to 1 (average 0.5) at a period of 1.5 s $\triangledown$. The dash line is a power law fit with exponent 0.7.

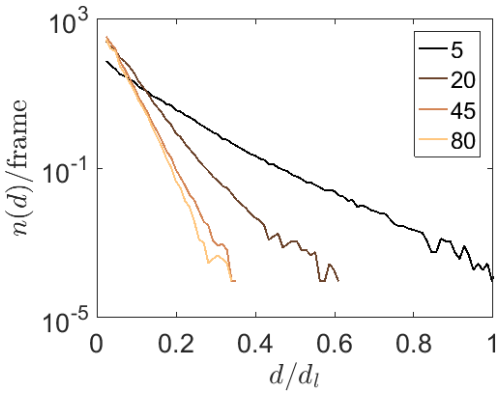

Figure 4. Histogram of the droplet size, normalized by the number of frames in the shadowgraph movies, for different momentum ratio M.

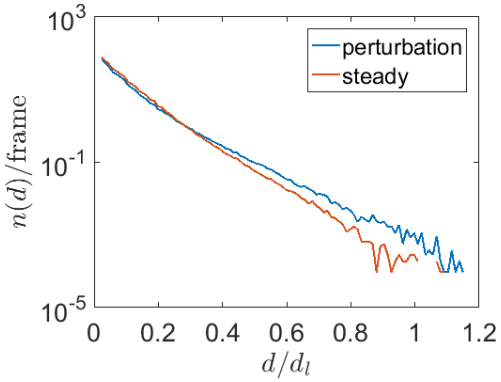

Figure 5. Histogram of the droplet size for a swirl ratio $SR = 0.5$ and for a swirl ratio modulated from 0 to 1 (average 0.5) at a period of 1.5 s, at a constant momentum ratio $M = 5$.

ondary break-up due to a lack of spatial resolution, quantitative analysis of the visualizations serves as a good estimate of the amount of liquid that is partially atomized after the primary break-up instability. This metric has the additional objective of comparing the quantitative information from optical visualizations with the same information extracted from x-ray attenuation by spray captured in high speed video at Argonne National Lab [4, 6] and at our collaborators at Iowa State University [5]. Droplets are detected when they are in focus and above a certain threshold, and we considered an object to be a drop when its diameter is smaller than the liquid diameter and its shape meets certain sphericity criterion. Droplet sizes are measured from all the image frames collected for each condition, and the histogram obtained is normalized by the total number of frames where droplets are detected (figure 4). The droplet size distributions are well approximated by a decaying exponential function, with the rate of decay increasing as M increases. This is consistent with the mechanism by which drops are atomized into finer droplets by the Rayleigh-Taylor instability at higher acceleration rates associated with larger gas drag on the liquid. Figure 5 shows the comparative effect of the swirl fluctuation in comparison to steady swirl. A higher proportion of large drops is seen, which translates into less fine droplets in the spray. This is in agreement with the stabilizing effect of harmonic fluctuations on the primary break-up instability seen with the flapping frequency behavior.

The accuracy of the droplets detection on the movies, in combination with the high acquisition frequency, allows for 2D tracking of the droplets that is sufficiently accurate to compute droplet acceleration (figure 6). Measuring the droplet acceleration distributions is not only useful to quantify the aerodynamics forces acting on them, but can also because it can be used to characterize the effect on an external force acting of the cloud of

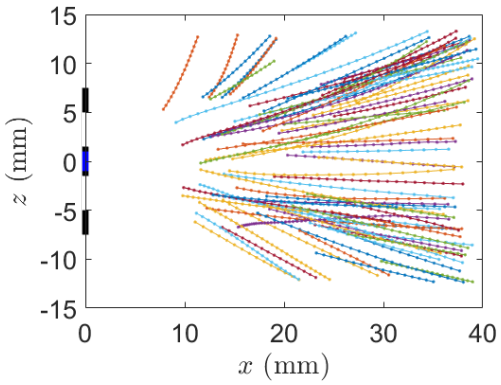

Figure 6. Subset of droplet trajectories obtained from the shadograph for a momentum ratio $M = 2.3$.

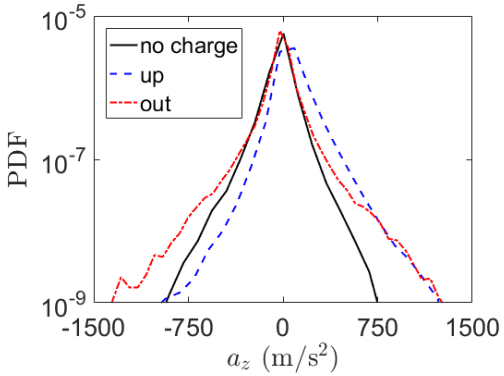

Figure 7. Probability density functions (PDF) of the vertical droplet acceleration in the absence of charge in the liquid (−), with an upward forcing (−−) and with an outward forcing (−.).

droplets, namely in the presence of the external electric field imposed by the streamwise plates on the charged liquid droplets. Figure 7 shows the droplet vertical acceleration probability density functions (PDF) without external force (except for gravity) and when the electrostatic external force is pointing upwards or outwards, perpendicular to the jet axis for $M = 2.3$. In the presence of the upward forcing, the PDF is both shifted in the mean towards positive values (by about 100 m/s^2) and skewed toward positive values with a skewness (i. e. centered and normalized third order moment) value of 1.3. For a radially outward force field, the mean acceleration stays equal to the non-charged one (equal to gravity downwards) while wider tails are observed for the probability distribution, with the standard deviation increased by 30% over the non-charged case.

Summary and Conclusions

We have demonstrated several open-loop control mechanisms deployed on a canonical coaxial two-fluid atomizer. In particular, while adding a certain amount of swirl to the gas can favor the primary break-up mechanism, we have quantified how low-frequency modulation of the swirling motions in the gas co-flow tends to stabilize this instability. Future work will characterize how the effects of this modulation vary with the momentum ratio and will consider high-frequency (ultrasonic) modulation of the fluid inlets.

We have shown that the presence of an external electric field can be used to tune the droplet spatial distribution of a spray when the liquid used is charged during injection. Large changes in the droplet acceleration distributions have been demonstrated. Future work will involve the characterization of the effective force on the droplets for different liquid mass loading and gas-to-liquid momentum ratio and how this force can change locally due to screening and other non-linear effects cause by neighboring charged droplets. Other external perturbations, such as an external acoustic field or high-speed perturbation of the liquid core, are also being implemented.

Acknowledgements

This work was sponsored by the Office of Naval Research (ONR) as part of the Multidisciplinary University Research Initiatives (MURI) Program, under grant number N00014-16-1-2617. The views and conclusions contained herein are those of the authors only and should not be interpreted as representing those of ONR, the U.S. Navy or the U.S. Government.

References

[1] Hopfinger, E. J., Lasheras, J. C., *Physics of Fluids* 8(7):1696-1698 (1996).
[2] Baillot, F., Blaisot, J. B., Boisdron, G., Dumouchel, C., *Journal of Fluid Mechanics* 640:305-342 (2009).
[3] Huck P., Machicoane N., Osuna R., Aliseda A., *14th Triennial International Conference on Liquid Atomization and Spray Systems*, Chicago, Illinois, July 22-26, 2018.
[4] Bothell, J. K., Li, D., Morgan, T. B., Heindel, T. J., Aliseda, A., Machicoane, N., Kastengren, A., *14th Triennial International Conference on Liquid Atomization and Spray Systems*, Chicago, Illinois, July 22-26, 2018.
[5] Li, D., Bothell, J. K., Morgan, T. B., Heindel, T. J., Aliseda, A., Machicoane, N., Kastengren, A., *14th*

Triennial International Conference on Liquid Atomization and Spray Systems, Chicago, Illinois, July 22-26, 2018.

[6] Morgan, T. B., Bothell, J. K., Li, D., Heindel, T. J., Aliseda, A., Machicoane, N., Kastengren, A., *14th Triennial International Conference on Liquid Atomization and Spray Systems*, Chicago, Illinois, July 22-26, 2018.

[7] Vu, L. X., Chiodi, R., Desjardins, O. *14th Triennial International Conference on Liquid Atomization and Spray Systems*, Chicago, Illinois, July 22-26, 2018.

[8] Varga, J. C., Hopfinger, E. J., Lasheras, J. C., *Journal of Fluid Mechanics*, 497:405-434 (2003).

[9] Marmottant, P. , Villermaux E., *Journal of Fluid Mechanics* 498:73-111 (2004).

[10] Lasheras, J. C., Hopfinger, E. J., *Annual Review of Fluid Mechanics*, 32:275-308 (2000)

[11] Aliseda, A., Hopfinger, E. J., Lasheras, J. C., Kremer, D. M., Berchielli, A., Connolly, E. K., *International Journal of Multiphase Flow* 34(2):161-175 (2008).